DESIGN AND MANUFACTURE OF NEW STIRLING ENGINE DISC HEATER

by

Jie Chai[1], Xiaohong Yang[1, 2, 3, *], Yunsong Li[1], Xiaoyu Gao[1] , Yongchao Quan[1]

[1]College of Energy and Power Engineering, Inner Mongolia University of Technology, Hohhot, P.R. China

[2]Key Laboratory of Wind Energy and Solar Energy Utilization Technology, Ministry of Education, Hohhot, P.R. China

[3] Inner Mongolia Autonomous Region New Energy Productivity Promotion Center, Hohhot, P.R. China

[*] Corresponding author: yxh1109@imut.edu.cn

The Stirling engine heater is a key component between the external heat source system and the working circulation system, which drives the piston by transmitting heat energy to the working gas. In this study, based on the U-shaped tube heater, a disc heater was designed and manufactured, and the average photothermal conversion efficiency reached 56.58% under outdoor conditions. The heat flux distribution of the two heaters at the same solar normal direct irradiance of 1000W/m^2 was compared using TracePro optical simulation software. The results show that the average heat flux density of the disc heater (2.083×10^{3}W/m^2) is more uniform than that of the U-shaped tube heater, and the effective radiation area is larger, which verifies the rationality of the design of the disc heater.

Key words*: Disc heater; Normal direct irradiance; TracePro； Heat flux density;*

1. Introduction

The direct utilization of solar energy is generally divided into three types: photothermal power generation, photovoltaic power generation, and hybrid power generation [1-3]. The solar photothermal power generation industry is rapidly developing [4]. The main forms of photothermal power generation systems include linear Fresnel, tower, trough, and dish types [5-8]. Solar dish power generation systems have attracted much attention for their high efficiency, low carbon emissions, and energy application flexibility [9]. The Stirling engine, an integral component of the dish thermal system, offers advantages such as low pollution, noise, fuel consumption, and adaptability to various heat sources [10-12]. It consists of five main components: heater, cooler, hot cavity, cold cavity, and regenerator [13]. Figure 1 demonstrates the working gas compression in the Stirling engine's cold chamber, followed by expansion in the hot chamber and the conversion of heat into work through the piston. The heater acts as a connecting component between the external heat source system and the work cycle system. Increasing the temperature enhances the power and efficiency of the Stirling engine [14]. The continuous heat demand of the Stirling engine and the working gas's temperature

depend on the heater's thermal performance [15]. Therefore, studying the performance of the Stirling engine heater holds great significance as it largely determines the engine's power generation efficiency [16-18].

Heaters in Stirling engines are mainly categorized into two types according to their shape: tubular heaters and finned heaters [19, 20]. Rabhi et al. [21] studied the above two types of heaters, the number and length of the tubes correspond to the fins. The study found that the tube heater increases the exchange area with the working gas, thus promoting the heat transfer between the heater and the working gas [22]. Li [23] designed a tubular heater for a one kW β-type Stirling engine, the CFD software is used to compare the tube heater and the fin heater. The tube heater is superior to the fin heater in terms of unprofitable volume, total heat transfer, and heat flux. Liu [24] designed an involute heat-absorbing tube cluster heater with 28 heating tubes and a length of 31 cm. The results show that the heater structure avoids the secondary flow of the working gas in the tube and reduces the pressure loss of the working gas in the heat absorption tube. For the Stirling engine at the same speed, the heat loss of the tube bundle is lower than that of the fin type [21]. The tube heat exchanger has the advantages of relatively good heat transfer performance and small dead volume. This allows the working gas to quickly and effectively absorb solar radiation energy and supply heat to the heater tube [25-27]. Luo [28] designed a tube heater with a diameter of 2 mm, a length of 40 mm, and several 288 heat exchange tubes arranged in a staggered arrangement. The results show that the total heat transfer coefficient of a single heat exchange tube can reach 2.38107 W/m^2. For Stirling generators of kilowatt level and above, a tube heat exchanger with good heat transfer performance and relatively small dead volume is selected. Therefore, tube heaters are commonly used in Stirling engines.

U-shaped tube heaters have greater heat transfer than straight-tube heaters [29], and the Stirling engine heating tubes used in most experiments are U-shaped. Scollo et al. [30] found that the heat transfer area of the Stirling engine heater is insufficient. To enhance the efficiency of the heater, it is necessary to increase the temperature and heat transfer rate of the heater tube by adding more heat transfer surfaces. For U-shaped heaters, the outer surface area can be increased by changing the shape of the tube. In the external heating system of the heater, especially under outdoor conditions, the solar irradiation has uncertainty and spot unevenness, which leads to the uneven distribution of heat flow on the surface of the heat tube. When the heat tube is unevenly heated, it will be damaged to different degrees [31] and is easily prone to air leakage when working for long periods of time.

Through the above analysis, based on the U-shaped tube heater of the Stirling engine, a disc heater is designed and manufactured. By controlling the structure of the elbow tube, the heating tube is arranged in a circular shape, thereby increasing the contact area between the solar radiation and the heat tube. The heat flux distribution of the two heaters under the same normal direct irradiance was simulated by simulation, and the influence of different normal direct irradiance on the thermal performance of the disc heater was studied in the outdoor test.

2. Introduction of the experimental system

2.1. Geometry description

Regarding the choice of tube diameter, smaller diameters lead to shorter inlet lengths and thicker boundary layers, thereby reducing the heat transfer rate of the tube. Studies have demonstrated that within the range of 2-5mm tube diameter, the impact of increasing both diameter and length on

the efficiency of the Stirling engine is nearly negligible [21, 28, 32]. For the selection of the number and shape of the tubes, the optimal number of heat-absorbing tubes N=28 [24, 33] is determined based on structural parameters. Figure 2 shows the arrangement of the heat tube of the disc heater. Considering that copper has good thermal conductivity and a higher melting point, copper is selected as the heat-absorbing tube material. The heat tube's copper tube has an outer diameter of 5 mm and an inner diameter of 4 mm.

To increase the heat absorbing area of the heater, and make the tube heated evenly. It is bent using a tube bender, expanding at 30° to the horizontal plane. The heat-absorbing tube consists of three layers: inner, middle, and outer. The inner and middle layers each contain 7 heat-absorbing tubes, while 14 are in the outer layer. The three-layer heat-absorbing tubes are evenly distributed along the circumferences. The diameters of the tubes in the three layers are 20, 34, and 46 mm, respectively. In addition, there are 28 heat-absorbing tubes connected to the regenerative cavity in the outer layer. These tubes are evenly distributed along a circumference of 72 mm. It is very convenient to process the heater when the tube is welded to the cavity. The specific design parameters are shown in Tab. 1.

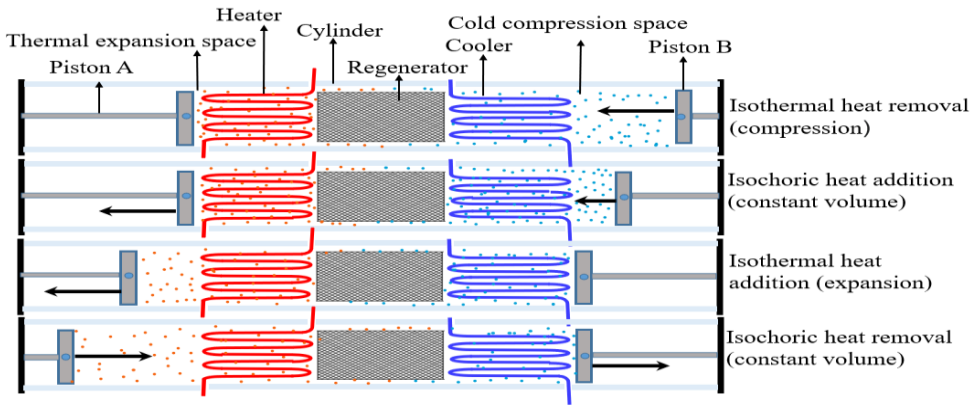

Figure 1. Stirling engine equipment system and working process

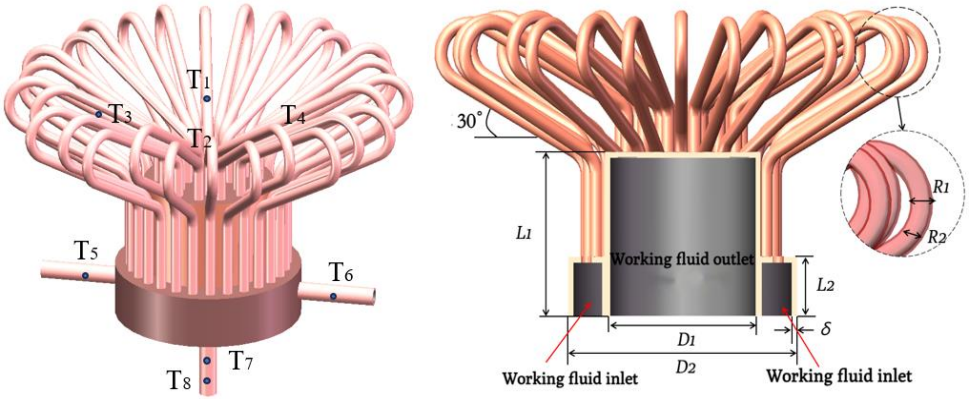

Figure 2. Schematic diagram of heater design and processing

Table 1. Disc heater design parameters

Parameters	Value	Parameters	Value
Expansion cavity height L_1 [mm]	40	The wall thickness of the cavity δ [mm]	2
The internal diameter of the expansion chamber D_1 [mm]	56	U-shaped tube bending radius R [mm]	11.5
Regenerative cavity high L_2 [mm]	20	Tube outer diameter D_{h2} [mm]	5
Regenerative cavity outer diameter D_2 [mm]	86	Tube inner diameter D_{h1} [mm]	4
Working gas volume V_{gas} [cm^3]	259.6	Number of tube roots	28
Heater height [mm]	92.6	Heater width [mm]	184.3
Inner ring single tube length [mm]	214	Length of the single tube in the middle ring [mm]	215
Length of outer ring single root canal [mm]	216.5	Tube wall thickness δ_h [mm]	0.5

2.2. Experimental system

Figure 3(a) shows the experimental system for dish solar photothermal conversion. To minimize energy loss, the disc heater is enclosed within a stainless steel insulation chamber. The inner and outer surfaces of the insulation cavity are wrapped with aluminum silicate wool, which is resistant to high temperatures (1400°C) and has a low thermal conductivity. An ultra-white glass optical window, 3mm thick, is installed at the front opening of the thermal insulation cavity. The heater is installed on the collector to absorb solar radiation energy and convert it into heat.

The heat is transferred from the outer wall of the heat absorption tube to the inner wall of the tube through heat conduction, and the circulating working gas is heated by convective heat transfer. During the test, the input normal direct irradiance constantly fluctuates, and the tube wall temperature and outlet temperature of the working gas in the heater are significant indicators for assessing its thermal performance. Before conducting the experimental test, two tasks should be completed: detecting and correcting the thermocouple to ensure accurate test temperature measurements, and performing a spot test to determine the actual position of the collector focus.

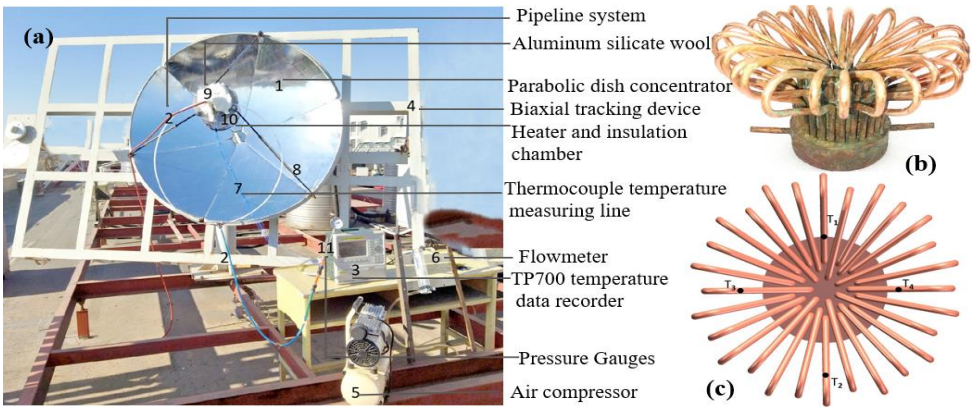

Figure 3. Physical diagram of the experimental test system

2.2.1 Thermocouple correction

As shown in Fig. 2 and Fig. 3(c), four thermocouples (T1-T4) of different lengths are arranged on the light-receiving surface of the heater, while one thermocouple is placed at each of the two inlet ends (T5-T6). The outlet arrangement of two thermocouples (T7-T8) yields measurement results that are recorded as the average value. Considering the safety of the experiment, thermocouples (T9) were arranged at the bottom of the ultra-white glass cover plate. Immersion of thermocouple contacts in a thermostatic water tank and the temperature of these nine thermocouples was measured using a standard mercury thermometer. The measured data are used to plot the calibration curve (Fig. 4). In the experiment, the temperature value is adjusted and fitted according to the calibration curve to obtain accurate results.

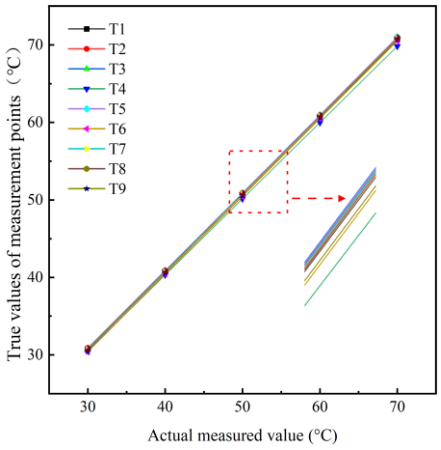

Figure 4. Thermocouple temperature fitting correlation diagram

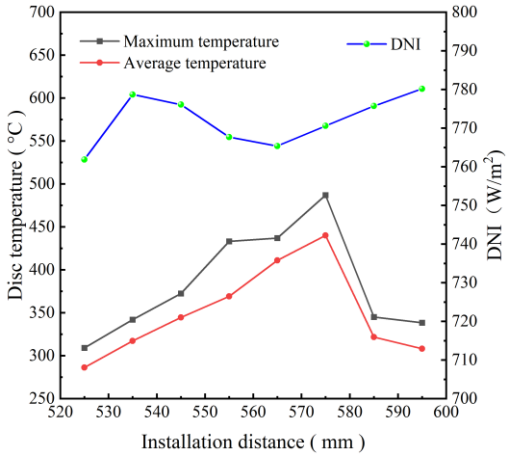

Figure 5. Disc temperature changes with installation distance

2.2.2 Focal plane distance test

To determine the optimal installation position of the heater, a high temperature-resistant disc is used as a substitute. The disc is moved vertically at the theoretical focal length of 555 mm, with an adjustment distance of 10 mm. A total of 8 sets of tests were performed, with a test range of 525-595 mm. The temperature distribution of each group of disc focal planes was photographed by an H36 infrared thermal imager at different times.

According to the results of Fig. 5 and Fig. 6, with the increase in installation distance, the maximum temperature and average temperature of the center point show a trend of increasing and then decreasing. At the distance of 575 mm, the temperature reaches the highest point, the average temperature is 439.9 °C, the highest temperature is 486.9 °C, and the focal spot shape is the most uniform. Therefore, in the subsequent experiments, the heater should be fixed at a distance of 575 mm from the collector.

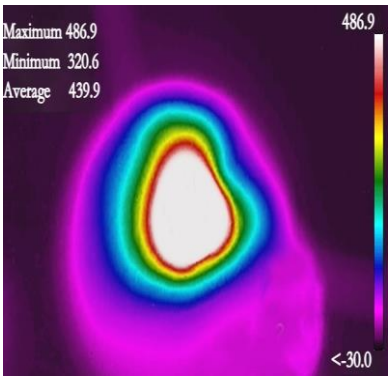

Figure 6. Infrared image of the temperature field of the disc focal spot (installation distance S=575mm)

2.3. Performance indicators

The collector is used to focus the solar energy, and the light is reflected to the disc heater by point focusing.This requires taking into account the reflectivity of the collector and the transmittance of the ultra-white glass of the receiver. Since the previous work has successfully insulated the heater, this study does not address heat conduction, heat convection, or radiation loss. For further information on the total solar radiation power captured by the collector, refer to [34-36].

$$Q_{in} = \rho \cdot \tau \cdot \bar{I} \cdot A_e \quad (1)$$

where ρ is the collector's specular reflection rate, τ is the transmittance of ultra-white glass, $\bar{I}$ is the average solar normal direct irradiance, and A_e is the effective reflective area(1.601m^2), The power obtained after the working gas air absorbs the heat energy of the tube wall is calculated by the following formula :

$$Q_a = c_p \cdot q_m \cdot (t_{out} - t_{in}) \quad (2)$$

c_p is the specific heat capacity of the working gas air, q_m is the mass flow rate of the working gas air, t_{out} and t_{in} are the outlet and inlet temperatures of the air, respectively.

Assuming that the input power of the system is constant, the ratio of the output power of the heater to the input power of the system is characterized as the thermal efficiency of the heater. The thermal efficiency of the system and the photothermal conversion efficiency of the heater are :

$$\eta_s = \frac{c_p \cdot q_m \cdot (t_{out} - t_{in})}{\bar{I} \cdot A_e} \quad (3)$$

$$\eta_h = \frac{c_p \cdot q_m \cdot (t_{out} - t_{in})}{\rho \cdot \tau \cdot \bar{I} \cdot A_e} \quad (4)$$

3. Results and discussion

3.1. Simulation of the optical performance

The Monte Carlo ray tracing is a calculation method grounded in probability and statistical theory [37]. It enables the sampling and analysis of specific light source distributions, as well as the simulation of complex light phenomena such as diffraction and scattering. A three-dimensional model of the disc heater and collector was constructed utilizing SolidWorks. In TracePro, the heat tube's

absorption rate for the heater is configured as 90%, while the concentrator's specular reflection rate is set to 90%. The simulation uses a grid light source for the illumination, and the solar incident angle is set at 0°. The heat flux distribution characteristics of the outer wall of the disc heater's heat tube were analyzed using TracePro optical simulation software. According to the theoretical focal length of the collector (555 mm [33]), adjust the distance between the top of the disc heater and the bottom of the collector to 555 mm. To ensure high calculation accuracy, the number of rays is set to be 3×10^6. Figure 7(a) shows the sampling ray tracing of the heater, and Fig. 7(b) shows a front view of the heater's irradiated rays, where the number of rays shown is 0.02% of the total.

The study explores the heat flux distribution of the disc heater and the U-shaped tube heater [38] under a normal direct irradiance value of 1000 W/m^2 (Fig. 8). The disc heater exhibits a maximum heat flux density of 3.98×10^4 W/m^2, a minimum value of 0.1469 W/m^2, and an average value of 2.083×10^3 W/m^2.The maximum heat flux density of the U-shaped tube heater is 1.9204×10^5 W/m^2, the minimum value is 0.1013 W/m^2, and the average value is 1.005×10^4 W/m^2.

As sunlight propagates linearly, the U-shaped tube heater experiences its highest irradiance at the bend of the tube. Consequently, the temperature of the outer wall in the curved section of the heater increases significantly. Localized temperature increases can lead to cracking of the tube wall, affecting its pressure capacity. In contrast, the disc heater has a more uniform surface heat flux distribution. The numerical fluctuation range is small, and the maximum heat flow of each heat tube is basically the same. Under the same light source intensity, although the high surface heat flux density of the U-shaped tube heater is larger, the effective radiant area of the heat-absorbing tube of the disc heater is larger. This is consistent with the purpose of designing a disc heater, which increases the outer surface area of the tubes and has a more uniform surface heat flow density distribution.

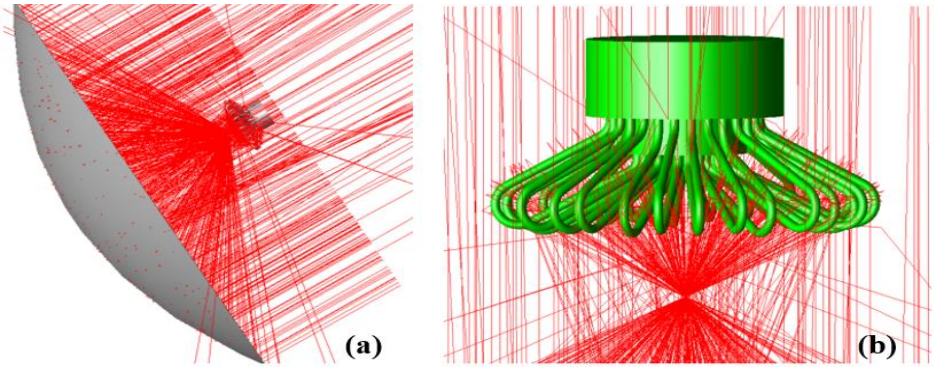

Figure 7. Heater irradiation ray tracing diagram

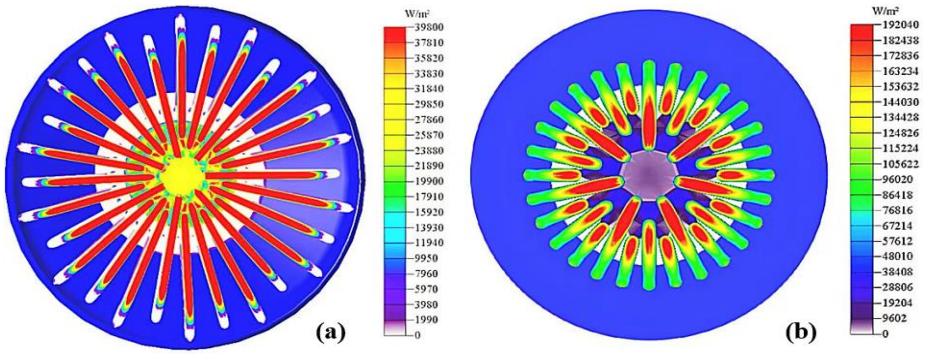

Figure 8. Heater energy flow distribution diagram (a) Disc type (b) U-shaped tube type

3.2. Effect of irradiance on tube wall temperature

The effect of normal direct irradiance on the wall temperature of the heater was tested under outdoor conditions, setting the distance between the heater and the collector to 575 mm. The experimental conditions are shown in Tab. 2.

Table 2. List of experimental conditions under different irradiation

Condition number	Condition 1	Condition 2	Condition 3
Initial normal direct irradiance [W/m^2]	317.64	400.91	691.92
Terminate normal direct irradiance [W/m^2]	376.18	468.07	620.44
Flow rate (L/h)	40	40	40
Average ambient temperature [℃]	-11.10	-10.27	-2.86
Average wind speed [m/s]	1.79	1.03	1.09

Figure 9(a) shows that during the initial stage of heat absorption (within 20 s) in condition 1, the tube absorbs radiant energy, converts it into heat energy, and then transfers the heat to different parts of the heater. This process takes some time, resulting in a gradual increase in temperature. As the overall temperature of the heater increases, heat loss from the surface of the heat tube increases, resulting in a lower rate of temperature rise. In Fig. 9(b), the normal direct irradiance drops abruptly between 16:45 and 16:47 due to cloud cover. However, the wall temperature has not shown a significant downward trend and the heating rate has decreased. This is because the heater exhibits thermal inertia, causing a lag in the internal temperature response to changes in normal direct irradiance. As a result, variations in normal direct irradiance have minimal impact on the temperature of the tube wall. Consequently, the wall surface continues to absorb solar radiation energy, leading to a steady rise in the temperature at the measuring point. By 16: 48, the input heat absorbed by the tube becomes limited, and the excess heat is distributed around. The heater is gradually in a state of thermal equilibrium.

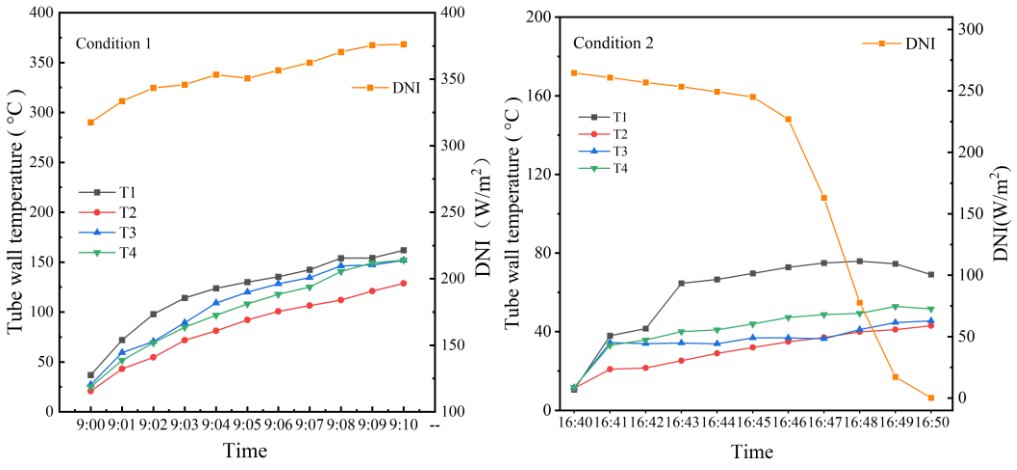

(a) **(b)**

Figure 9. Curves of normal direct irradiance and tube wall temperature changing with time in working conditions 1 and 2

3.3. The influence of irradiance on the working gas

The heater's air outlet temperature and flow rate were measured to observe its variation with normal direct irradiance. Referring to Fig. 10 (a) and Section 2.2, the outlet air temperature continues to rise despite a gradual decrease in normal direct irradiance and a lower heating rate. As shown in Fig. 10(b), the airflow rate reached a maximum of 40 L/h during the initial heating stage of condition 3. As the heat tube temperature increases, the air expansion causes the flow rate to decrease. The airflow in the heater is driven by differential pressure. When the tube is heated by solar radiation, the air temperature rises, increasing viscosity and flow resistance. Consequently, the pressure difference between the inlet and outlet of the heater rises. Given a constant outlet-rated pressure of the air compressor, the airflow resistance is inversely proportional to the airflow rate. Overall, the airflow demonstrates a fluctuating downward trend. This trend is attributed to the uncertainty in the normal direct irradiance change, which affects the outlet temperature. At certain points, the air outlet temperature decreases, resulting in reduced flow resistance and an increase in flow rate.

For this study, changes in the temperature of the tube wall and outlet working gas for disc heaters are important indicators of thermal performance. The analysis of the aforementioned results reveals that the temperature change at the measuring point and the outlet temperature of the working gas align with the anticipated expectations.

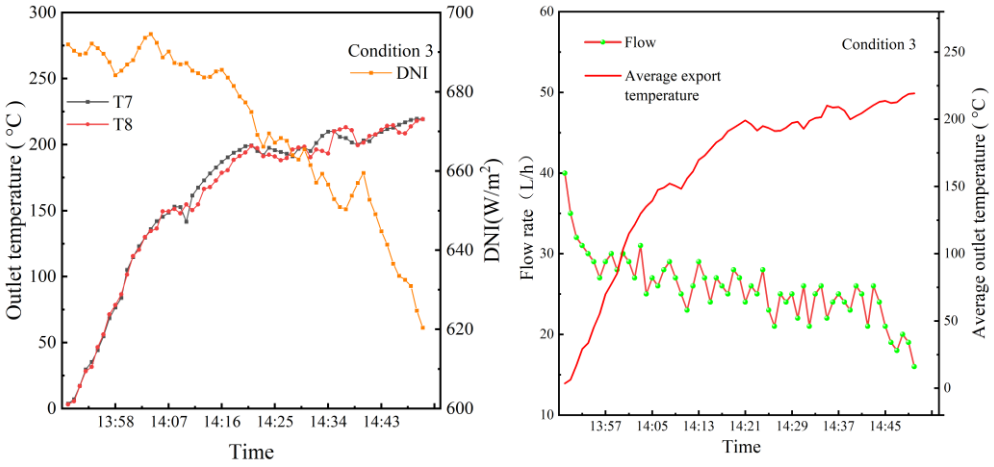

(a) **(b)**

Figure 10. Changes in heater outlet temperature and airflow with time

3.4. Analysis of Photothermal Conversion Efficiency

During the test period of condition 3, normal direct irradiance generally showed a steady downward trend. As shown in Fig. 11, the overall trend of photothermal conversion efficiency, thermal efficiency, and thermal power is the same as normal direct irradiance. During the test, the average photothermal conversion efficiency of the heater under condition 3 was 56.58%, the average photothermal efficiency was 47.81%, and the average thermal power was 445.33 W. Limited by the change of environment, the thermal efficiency and thermal power of the heater are multi-peak and fluctuate greatly near the peak. The irradiation loss and convective heat loss are consistent with the decreasing trend of normal direct irradiance, which improves the heat absorption efficiency of the heater. A curved heat pipe cushions sudden changes in efficiency from varying with power. It also

compensates for sudden changes in incident power over a short period of time. Therefore, there is a hysteresis in the thermal power. Generally, thermal efficiency and thermal power increase together.

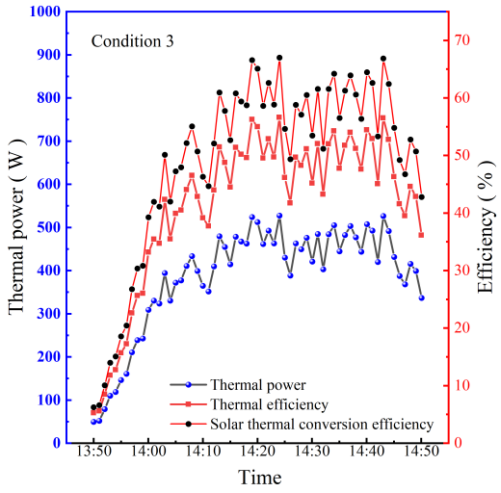

Figure 11. Relationship between thermal efficiency and thermal power over time

4. Conclusion

In this study, a disc heater based on the U-shaped tube heater is designed and manufactured. Using TracePro optical simulation, the heat flux distribution characteristics of heaters were simulated under a normal direct irradiance value of 1000 W/m^2.The results indicate that the disc heater has a maximum heat flux density of 3.98×10^4 W/m^2, whereas the U-shaped tube heater has a maximum heat flux density of 1.9204×10^5 W/m^2. The disc heater exhibits a more uniform heat flux distribution and a larger surface area compared to the U-shaped tube heater. These characteristics are critical for the heater's lifespan and the stable operation of the Stirling engine. The disc heater has an average photothermal conversion efficiency of 56.58%, an average photothermal efficiency of 47.81%, and an average thermal power of 445.33 W. However, these results solely evaluate the thermal performance of the heater individually, and the installation of the heater in the Stirling engine is necessary for further testing.

Acknowledgment

This work was supported by Inner Mongolia Autonomous Region Natural Science Foundation Project, China [No. 2023MS05014]; Program for Innovative Research Team in Universities of Inner Mongolia Autonomous Region [No. NMGIRT2309]; Industrial Technology Innovation Project of Inner Mongolia Academy of Science and Technology [No. 2023JSYD01001].

Nomenclature

c_p	- specific heat, [Jkg^{-1}K^{-1}]	*Subscripts*	
$\overline{I}$	-average solar normal direct irradiance, [Wm^{-2}]	*a*	-air
q	-mass flow, [gs^{-1}]	*h*	-heater
Q	-power, [W]	*in*	-inlet
t	- temperature, [℃]	*m*	-mass

Greek symbles		*out*	-outlet
η	-efficiency, [%]	*s*	-system
τ	-penetration rate, [-]		
ρ	-density ,[kgm^{-3}]		

References

[1] Saberi, Z., *et al*., Performance assessment of double pass photovoltaic/thermal solar air collector using bifacial PV with CPC and mirror reflector under Malaysian climate, *Case Studies in Thermal Engineering, 44* (2023), pp. 102811, DOI: 10.1016/j.csite.2023.102811

[2] Razali, N. F. M., *et al*., Review of water-nanofluid based photovoltaic/thermal (PV/T) systems, *International Journal of Electrical and Computer Engineering, 9* (2019), 1, pp. 134, DOI: 10.11591/ijece.v9i1

[3] Yadav, V. K., *et al*., Thermodynamic, economic and environmental analyses of novel concentrated solar-PV-thermal integrated combined power, cooling and desalination system, *Desalination, 563* (2023), pp. 116721, DOI: 10.1016/j.desal.2023.116721

[4] S., M., *et al*., A review on solar energy use in industries, *Renewable and Sustainable Energy Reviews, 15* (2010), 4, pp. 1777-1790, DOI: 10.1016/j.rser.2010.12.018

[5] de Sá, A. B., *et al*., Experimental study of a linear Fresnel concentrator: A new procedure for optical and heat losses characterization, *Energy, 232* (2021), pp. 121019, DOI: 10.1016/j.energy.2021.121019

[6] Chen, J., *et al*., Experiment and dynamic simulation of a solar tower collector system for power generation, *Renewable Energy, 196* (2022), pp. 946-958, DOI: 10.1016/j.renene.2022.07.045

[7] Wang, Q., *et al*., A hybrid parabolic trough solar collector system integrated with photovoltaics, *Applied Energy, 329* (2023), pp. 120336, DOI: 10.1016/j.apenergy.2022.120336

[8] Allouhi, H., *et al*., Recent advances, challenges, and prospects in solar dish collectors: Designs, applications, and optimization frameworks, *Solar Energy Materials and Solar Cells, 241* (2022), pp. 111743, DOI: 10.1016/j.solmat.2022.111743

[9] Islam, R., *et al*., An Overview of Concentrated Solar Power (CSP) Technologies and its Opportunities in Bangladesh, *2017 International Conference On Electrical, Computer and Communication Engineering (Ecce)* (2017), pp. 844-849, DOI:10.1109/ECACE.2017.7913020

[10] F., F., *et al*., Analytical model for Stirling cycle machine design, *Energy Conversion and Management, 51* (2010), 10, pp. 1855-1863, DOI: 10.1016/j.enconman.2010.02.010

[11] Zhengchang, S., *et al*., Heat transfer enhancement in tubular heater of Stirling engine for waste heat recovery from flue gas using steel wool, *Applied Thermal Engineering, 87* (2015), pp. 499-504, DOI: 10.1016/j.applthermaleng.2015.05.028

[12] S., C. C., *et al*., Numerical study of the pressure drop phenomena in wound woven wire matrix of a Stirling regenerator, *Energy Conversion and Management, 67* (2013), pp. 57-65, DOI: 10.1016/j.enconman.2012.10.014

[13] Salih, S. A., *et al*., Isothermal thermodynamic analysis investigation of the Stirling engine types (alpha, beta, gamma): A theatrical study, *Materials Today: Proceedings* (2023), DOI: 10.1016/j.matpr.2023.03.069

[14] Sharma, A., *et al*., FINITE TIME THERMODYNAMIC ANALYSIS AND OPTIMIZATION OFSOLAR-DISH STIRLING HEAT ENGINE WITH REGENERATIVE LOSSES, *Thermal Science, 15* (2011), 4, pp. 995-1009, DOI: 10.2298/TSCI110418101S

[15] R., G., *et al*., Experimental and theoretical investigation of Stirling engine heater: Parametrical optimization, *Energy Conversion and Management, 105* (2015), pp. 285-293, DOI: 10.1016/j.enconman.2015.07.063
[16] Naotake, H., *et al*., Improvement in Specific Power of Stirling Engine by Using a New Heat Exchanger, *Journal of the Japan Institute of Energy, 88* (2009), 12, pp. 1095-1100, DOI: 10.3775/jie.88.1095
[17] Sun, D. M., *et al*., Design and experimental verification of a heater for themoacoustic heat engine, *JOURNAL OF ENGINEERING THERMOPHYSICS, 25* (2004), 02, pp. 226-228
[18] A., A. E., *et al*., Experimental investigation of the performance of an elbow-bend type heat exchanger with a water tube bank used as a heater or cooler in alpha-type Stirling machines, *Renewable Energy, 36* (2010), 2, pp. 488-497, DOI: 10.1016/j.renene.2010.07.011
[19] Gao, X.Y., *et al*., Numerical simulation on heat transfer enhancement of free piston Stirling engine heater with composite cross section mini channels, Numerical Heat Transfer, Part B: Fundamentals, *84* (2023), 3, pp. 294-314, DOI: 10.1080/10407790.2023.2202878
[20] Alfarawi, S., *et al*., Influence of phase angle and dead volume on gamma-type Stirling engine power using CFD simulation, *Energy Conversion and Management, 124* (2016), pp. 130-140, DOI: 10.1016/j.enconman.2016.07.016
[21] L Rabhi., *et al*., Examination of Stirling engine parameters effect on its thermal efficiency using PROSA software, *Thermal Science* (2023), 00, pp. 139-139, DOI: 10.2298/TSCI220617139R
[22] Gheith, R., *et al*., 4.6 Stirling Engines, in: *Comprehensive Energy Systems* (Ed. I. Dincer), Elsevier, Oxford, 2018, pp. 169-208
[23] Li, J. X., Design and Research of the Heater for the Small Scale Stirling Engine, M.Sc. thesis, Dalian University of Technology, Dalian, CHN, 2012 (in Chinese)
[24] Liu, F. M., *et al*., Design and Performance Simulation of Involute Cluster Tube Type Heat Absorber for Solar Stirling-engine, *(Journal of Hunan University of Science & Technology (Natural Science Edition)), 34* (2019), 01, pp. 54-63 (in Chinese)
[25] Çınar, C., *et al*., Manufacturing and testing of an α-type Stirling engine, *Applied Thermal Engineering, 130* (2018), pp. 1373-1379, DOI: 10.1016/j.applthermaleng.2017.11.132
[26] Z, M. F., *et al*., Thermodynamic performance prediction of rhombic-drive beta-configuration Stirling engine, *Iop Conference Series: Materials Science and Engineering, 469* (2019), 1, pp. 012048, DOI: 10.1088/1757-899X/469/1/012048
[27] Mazdak, H., *et al*., Enhancing and multi-objective optimising of the performance of Stirling engine using third-order thermodynamic analysis, *International Journal of Ambient Energy, 39* (2018), 4, pp. 382-391, DOI: 10.1080/01430750.2017.1303638
[28] Luo, X. K., *et al*., Design of a Tubular Heater for 1 kW Stirling Generator, *Vacuum and Cryogenics, 27* (2021), 05, pp. 467-472 (in Chinese)
[29] Ni, M., *et al*., Heat transfer characteristics of the oscillating flows of different working gases in U-shaped tubes of a Stirling engine, *Applied Thermal Engineering, 89* (2015), pp. 569-577, DOI: 10.1016/j.applthermaleng.2015.06.063
[30] Scollo, L. S., *et al*., Twin cylinder alpha stirling engine combined model and prototype redesign, *International Journal of Hydrogen Energy, 38* (2013), 4, pp. 1988-1996, DOI: 10.1016/j.ijhydene.2012.01.180
[31] Du, X. L., *et al*., Design and Research of Stirling Engine Heat Exchange Device, *Mechanical Engineering and Technology, 5* (2016), 4, pp. 382-390, DOI: 10.12677/MET.2016.54047 (in Chinese)

[32] Xiao, G., *et al*., Design optimization with computational fluid dynamic analysis of β-type Stirling engine, *Applied Thermal Engineering, 113* (2017), pp. 87-102, DOI: 10.1016/j.applthermaleng.2016.10.063
[33] Luo, G., Study on Photo Thermal Properties of Dish Solar Receiver, M.Sc. thesis, Inner Mongolia University of Technology, Hohhot, CHN, 2017 (in Chinese)
[34] Thombare, D. G., *et al*., Technological development in the Stirling cycle engines, *Renewable and Sustainable Energy Reviews, 12* (2008), 1, pp. 1-38, DOI: 10.1016/j.rser.2006.07.001
[35] Buscemi, A., *et al*., A validated energy model of a solar dish-Stirling system considering the cleanliness of mirrors, *Applied Energy, 260* (2020), pp. 114378, DOI: 10.1016/j.apenergy.2019.114378
[36] Hachicha, A. A., *et al*., A review study on the modeling of high-temperature solar thermal collector systems, *Renewable and Sustainable Energy Reviews, 112* (2019), pp. 280-298, DOI: 10.1016/j.rser.2019.05.056
[37] Dai, B., *et al*., Thermal performance of a directional heat radiation device utilizing the Monte Carlo ray tracing method, *Applied Thermal Engineering, 217* (2022), pp. 119257, DOI: 10.1016/j.applthermaleng.2022.119257
[38] Zhu, H., Numerical Simulation Study on Thermal Performance of Stirling Engine Tubular Heater, M.Sc. thesis, Inner Mongolia University of Technology, Hohhot, CHN, 2020 (in Chinese)

RECEIVED DATE: 9.7.2023.
DATE OF CORRECTED PAPER: 2.10.2023.
DATE OF ACCEPTED PAPER: 12.11.2023.